Analysis of a High Velocity Oxygen-Fuel (HVOF) Thermal Spray Torch, Part 1: Numerical Formulation*

DRAFT

William L. Oberkampf
Aerodynamics Dept., Org. 1554
Sandia National Laboratories
Albuquerque, NM 87185-0825

Milind Talpallikar
CFD Research Corporation
3325 Triana Blvd.
Hunstville, AL 35805

Abstract

The fluid and particle dynamics of a High Velocity Oxygen-Fuel (HVOF) torch are analyzed using computational fluid dynamic (CFD) techniques. The thermal spray device analyzed is similar to a Metco Diamond Jet torch with powder injection. The spray nozzle is axisymmetric with powder injection on the centerline, premixed fuel and oxygen fed from an annulus, and air cooling injected along the interior surface of the aircap. Choked flow conditions occur at the exit of the aircap and a supersonic, under-expanded jet develops externally. The CFD simulation assumes three injection streams (solid metal particles with argon as a carrier gas, premixed oxygen/fuel, and air) inside the aircap and solves the combusting two-phase flow until the external spray stream decays to sonic conditions. The numerical formulation solves the mass, momentum, and energy transfer for both the gas and particle phase and strongly couples each phase. The combustion process is modeled using approximate equilibrium chemistry with dissociation of the gas with a total of nine species. Melting and re-solidification of the metal particles is modeled as a lumped-mass system. Turbulent flow is modeled by a two equation k-ε turbulence model, including compressibility effects on turbulent dissipation. A time iterative, implicit, finite volume numerical method is used to solve the partial differential equations. A companion paper [10] presents the results of the numerical simulation and gives a detailed discussion of the gas and particle dynamics.

THERMAL SPRAYING using the High-Velocity Oxygen-Fuel (HVOF) process is being used in an increasing variety of coating applications. Metallic, ceramic and composite coatings are being applied to substrates to improve wear-resistance, abrasion resistance, thermal and electrical insulation, and corrosion protection. Coatings applied using HVOF spraying have proven to be of high density, good bond and mechanical strength, and a thermal expansion coefficient near the substrate material. HVOF spray torches use a combustion process to heat the gas flow and the coating material and then accelerate the gas/particle two-phase flow to high velocities. The gas and particle velocities are commonly much higher than those achieved using plasma spraying. The high

* Part of this work was performed at Sandia National Laboratories, which is operated by Martin-Marietta Corp. for the U. S. Department of Energy under contract No. DE-AC04-94AL85000.

DISCLAIMER

particle velocities are derived from two factors. First, HVOF torches normally produce supersonic external flows, whereas plasma torches normally operate with a subsonic stream. Second, gas density in HVOF torches is typically much higher than in plasma torches because their higher gas temperatures are much lower. The maximum gas temperature in HVOF spraying is typically 3,000 K, whereas in plasma spraying it is typically 10,000 K. The combination of high gas velocity and high density accelerate the spray particles to significantly higher speeds, thereby tending to produce higher density coatings.

There have been two experimental investigations to improve the physical understanding of the gas dynamics, chemistry, turbulence, and particle characteristics of HVOF spraying. Kowalsky, et al. [1] experimentally investigated the Flame-Spray Industries' CDS torch. This torch uses propylene and oxygen for combustion and a powder feed for particle injection. Velocities of alumina, tungsten carbide and tribaloy particles in the torch plume were measured using an L2F technique. Pressure measurements inside the torch and photographic measurements were made to determine various gas dynamic characteristics of the torch. Hackett, Settles, and Miller [2] recently investigated the external gas dynamics of the Hobart-Tafa JP-5000. This torch uses a liquid kerosene fuel injection system which atomizes the fuel and reacts with gaseous oxygen. They present an excellent description of the gas dynamics of the torch, particularly the free-jet mixing of the high temperature plume with the surrounding atmosphere.

The first quantitative analysis of the gas dynamics and particle dynamics of HVOF spraying was conducted by Thorpe and Richter [3]. They analyzed the internal and external flow of a newly designed HP/HVOF torch from Hobart TAFA Technologies, which is similar to the Union Carbide D-Gun®. They computed the energy release from an equilibrium chemistry model of heptane and oxygen, assuming no influence from the gas motion. They used one-dimensional isentropic flow assumptions to compute the flow through a converging/diverging section of the nozzle. One-dimensional flow assumptions were then used to compute the effect of friction (Fanno flow) in the constant diameter barrel of the torch. External to the torch they used linearized shock-expansion theory to calculate the under-expanded supersonic jet flow, ignoring mixing with the ambient air. Particle trajectories were also calculated, assuming no interaction with the gas stream.

More recent analyses have used modern computational fluid dynamic (CFD) methods to simulate more complex physics in two dimensions. Some of this improvement in modeling thermal spraying has been brought about by use of computational techniques developed for gas turbine engines and liquid and solid rocket motors. Axisymmetric and planar two-dimensional CFD simulations of chemically reacting, dissociated and ionized flows, along with state of the art turbulence models, has been presented in the literature. Researchers that have modeled thermal spray problems have used an Eulerian description of the gas flow and either an Eulerian or Lagrangian description of the dispersed phase, that is, the particles. Both the Eulerian-Eulerian formulation and the Eulerian-Lagrangian formulation compute the continuous phase, i.e., the gas, using an Eulerian approach. The influence of the particulate phase, either liquid or solid particles, on the continuous phase is accounted for by inclusion of interphase coupling terms in the Eulerian

equations. Some analyses, however, have completely ignored the coupling of the particulate phase and the gas phase. These simulations compute the effect of the flow on the particles but do not allow an effect of the particles on the flow. The particulate phase can be treated as either a continuous or a discrete model. In the Eulerian-Eulerian approach a similar description to the continuous phase is also used for the particulate phase. This model is sometimes referred to as the two-fluid model because the dispersed phase equations are similar to the continuum fluid dynamics equations. The Eulerian-Lagrangian approach employs a Lagrangian description of the particulate phase. A relatively small number of computational particles are used to model a large collection of physical particles, either solid or liquid. Each approach has it strengths and weaknesses, but it is generally believed that for modeling spray phenomena the Eulerian-Lagrangian approach is superior.

Ramshaw and Chang [4] modeled a thermal plasma using a two-dimensional CFD approach with extensive plasma physics. The plasma was modeled as a multicomponent, chemically reacting gas in local thermodynamic equilibrium. Ionization, dissociation, recombination, and other chemical reactions were computed by general kinetic equilibrium chemistry algorithms. No particulates were included in the simulation. Chang [5] used a similar computational approach to model alumina spraying in an argon-helium plasma jet. The plasma is represented as a continuous multi-component chemically reacting ideal gas with temperature-dependent thermodynamic and transport properties. These formulations, as are most techniques, solve the numerical equations with a time marching scheme until a steady state solution is achieved. The time marching technique, however, is an explicit scheme which requires very long computer run times when high spatial resolution is required.

Various investigators have used CFD techniques to model the spray forming, or spray casting, process. El-Haggar and Crowe [6] modeled the external two-phase flow including the stagnation of the flow on a flat substrate. They used a PSI-Cell (Particle-Source-In-Cell) method and a finite difference method to solve the coupled two-phase flow equations. The velocities were small at the nozzle exit and the temperature was relatively low so no compressibility or chemistry effects were considered. Berry, Gibeling, and de Jong [7] modeled the gas flow and liquid metal stream atomization inside a spray forming nozzle. They considered liquid metal injection from a slot at the throat of a converging-diverging nozzle for planar two-dimensional flow. They used a density based formulation for the gas phase and an implicit, time iterative, finite difference method to solve the equations. As with El-Haggar and Crowe, the gas temperature and flow velocities were low so that no chemistry effects were considered and the flow was essentially incompressible.

Power, Barber, and Chiappetta [8] and Smith, et al. [9] conducted the first CFD simulation of the HVOF spraying process. They modeled both the internal and external flow of the Metco Diamond Jet torch. In this torch, powder is fed through a center tube using nitrogen as a carrier gas. Premixed oxygen and propylene are injected through an annulus in the nozzle. This annulus is a simplification of the eight small holes in the nozzle to introduce pre-mixed fuel and oxygen. Air is

injected in an outer annulus in the nozzle for the purpose of cooling the aircap, as the torch has no other cooling mechanism. The combusting subsonic flow was modeled inside the converging aircap and the flow became choked at the exit of the aircap, that is, attained the sonic condition. External to the torch, they modeled the decay of the supersonic jet in a quiescent atmosphere. As the pressure in the torch was greater than atmospheric at the exit, the jet was under-expanded. The flow then expanded exterior to the aircap and formed "shock diamonds" commonly seen in supersonic under-expanded streams. Their CFD simulation included a k-ε turbulence model and combustion chemistry. Their chemistry model included dissociation of the reaction products using an approximate equilibrium model and seven gas species; C_3H_6, O_2, N_2, H_2O, CO_2, CO, and H_2. The finite difference equations, using a density based formulation, were solved by an explicit time iterative scheme. Particles of various sizes were injected inside the aircap near the centerline but these particles did not interact in any way with the gas stream. They were tracker particles responding to the local gas velocity and temperature but did not change the flow. Their analysis also did not account for any phase change of the particles.

The present paper presents the formulation and numerical methods of a CFD analysis of an HVOF torch geometry similar to the Metco Diamond Jet torch. A companion paper [10] presents the results of the numerical simulation and discusses the gas dynamics and particle dynamics of HVOF thermal spraying. The analysis uses an Eulerian-Lagrangian formulation for the gas and particle phases, respectively. A k-ε turbulence model is used which includes compressibility correction terms to account for the decrease in turbulent mixing that occurs for supersonic Mach numbers. Combustion is modeled by an approximate equilibrium chemistry model that accounts for dissociation of the combustion products. Dissociation strongly restricts the rise in the gas temperature because much of the thermal energy released from combustion is consumed in breaking the chemical bonds of the reactant species. Solid particles are introduced near the centerline of the aircap and are strongly coupled to the numerical solution of the gas phase. Mass, momentum and thermal energy are exchanged between the particulate phase and the gas phase. Solid particles are modeled as a lumped mass and those that attain the melting temperature change phase to liquid. Details of the mathematical and numerical modeling are given along with computer resources required to obtain the computational results.

Mathematical Modeling

The mathematical model of the flow physics will now be presented. The elements of the mathematical model are the torch geometry and the modeling of the gas phase, fluid dynamic turbulence, reacting flow chemistry, and liquid/solid particles. These elements of modeling are distinct topics separate from numerical modeling issues, that is, approximate mathematical representation of the continuum physics in terms of difference equations and the subsequent computer solution of these equations. Only a summary of the mathematical and numerical modeling will be given here. For more detailed information see, for example, Refs. 11 - 12. The mathematical and numerical model described in the present work is embodied in the computer code

CFD-ACE, which is commercially available from CFD Research Corp., Hunstville, Alabama.

Torch Geometry. The geometry chosen for the present analysis is similar to the Metco Diamond Jet torch, but there are notable differences. Figure 1 shows the detailed internal geometry of the conceptual torch analyzed. Although this geometry does not match precisely any existing torch design, it does represent an HVOF geometry that captures all of the important gas dynamic and two-phase flow features typical of HVOF spray torches. The conceptual torch is an axisymmetric, two-dimensional geometry, i. e., rotational symmetry is assumed. The central stream uses argon as the carrier gas to inject solid spherical particles of copper through a circular tube. The second stream injects premixed propylene and oxygen through an annulus at an angle of 5^{o} to the centerline. The third stream injects air through an annulus at an angle of 5^{o} adjacent to the wall for cooling of the aircap. The mass flow rate of each gas stream is specified, as is the mass flow rate and size of the spherical particles in the central stream. The aircap geometry is a 5^{o} half-angle, conically converging nozzle that attains a minimum area at a distance of 10 mm from the injection location. The torch is assumed to exhaust to ambient conditions consisting of air at room temperature and pressure. The only external boundary is the aircap exit plane which is assumed to extend radially outward.

The general character of the internal flow field is a release of thermal energy from the oxy-propylene combustion and a resulting increase in pressure inside the aircap. The premixed oxy-propylene stream is assumed to begin combusting as soon as it enters the computational domain. The combustion can also include oxygen from the adjacent air stream. The pressure is sufficient in the aircap to choke the flow through the nozzle exit, that is, Mach one is attained at the exit of the aircap. As the pressure in the exit plane is greater than the ambient condition, the air cap flow is said to be under-expanded. The flow will expand supersonically external to the nozzle so as to meet the ambient pressure condition. The external pressure adjustment of the supersonic stream occurs through a alternating series of expansion and compression waves. Certain portions of the compression waves coalesce into shock waves. The luminescence of the flow after these shock waves is normally referred to as "shock diamonds." The perimeter of the supersonic stream immediately begins turbulent mixing with the ambient air and, consequently, the gas velocity decreases. After several shock diamonds, the flow decays to subsonic conditions while entraining increasing amounts of cool ambient air. The numerical simulation terminates at an axial distance of 20 aircap radii from the exit plane, at which time the flow is entirely subsonic.

Gas Phase Modeling. The governing equations for the gas phase are the conservation of mass, momentum, and energy for unsteady, compressible, turbulent flow. These are written in Cartesian tensor form as:

$$\frac{\partial \bar{\rho}}{\partial t} + \frac{\partial\left(\bar{\rho}\tilde{u}_j\right)}{\partial x_j} = 0$$

$$\frac{\partial\left(\bar{\rho}\tilde{u}_i\right)}{\partial t} + \frac{\partial\left(\bar{\rho}\tilde{u}_i\tilde{u}_j\right)}{\partial x_j} = \frac{\partial \bar{p}}{\partial x_i} +$$

$$+\frac{\partial}{\partial x_j}\left[(\bar{\mu}+\mu_t)\left(\frac{\partial \tilde{u}_i}{\partial x_j}+\frac{\partial \tilde{u}_j}{\partial x_i}-\frac{2}{3}\frac{\partial \tilde{u}_m}{\partial x_m}\delta_{ij}\right)\right]-\frac{2}{3}\frac{\partial(\bar{\rho}k)}{\partial x_j}$$

$$\frac{\partial(\bar{\rho}\tilde{H})}{\partial t}+\frac{\partial(\bar{\rho}\tilde{u}_j\tilde{H})}{\partial x_j}=\frac{\partial}{\partial x_j}\left[(\bar{\Gamma}+\Gamma_t)\frac{\partial \tilde{H}}{\partial x_j}\right]+\frac{\partial}{\partial x_j}\left[(\bar{\mu}-\bar{\Gamma}+\mu_t-\bar{\Gamma}_t)\frac{\partial}{\partial x_j}\left(\frac{1}{2}\tilde{u}_k\tilde{u}_k\right)\right]+$$

$$+\frac{\partial \bar{p}}{\partial t}+\frac{\partial}{\partial x_j}\left[(\bar{\mu}+\mu_t)\tilde{u}_i\left(\frac{\partial \tilde{u}_i}{\partial x_j}+\frac{\partial \tilde{u}_j}{\partial x_i}-\frac{2}{3}\frac{\partial \tilde{u}_k}{\partial x_k}\delta_{ij}\right)\right]-\frac{2}{3}\frac{\partial \tilde{u}_k}{\partial x_k}\delta_{ij}$$

where (~) denotes Reynolds averaged, i. e., time averaged, quantities and (~) denotes Favre averaged, i. e., density averaged, quantities. ρ is the fluid mass density, u_i is the i-th Cartesian component of the velocity, and p is the static pressure. (The static pressure is that pressure experienced by a fluid element moving at the local gas velocity.) μ is the molecular (laminar) viscosity of the gas, μ_t is the turbulent, or eddy, viscosity and δ_{ij} is the Kronecker delta. H is the total enthalpy of the gas and is defined by $H = h + (u_j u_j)/2$ where h is the static enthalpy. Γ and Γ_t are the laminar and turbulent diffusivity coefficients, respectivley, and are defined as μ/σ and μ/σ_t. σ is the Prandtl number. The laminar viscosity and thermal conductivity are both functions of temperature.

The gas phase equations, as well as the turbulence model and particle trajectory equations, are transformed from physical space to computational space. This is done to fit, or map, the grid onto each surface in physical space. That is, a surface fitted grid in physical space is mapped to a square (for 2-D problems) or a cube (for 3-D problems) in computational space. This is done using an independent variable transformation of (x,r) to general non-orthogonal coordinates (ξ,η). The body-fitted-coordinate transformation technique is well known in the literature (see, for example, Ref. 13).

Turbulence Modeling. For turbulent flow, the Reynolds stress tensor is closed using the k-ε turbulence model of Launder and Spalding [14]. k is the turbulent kinetic energy and ε the rate of dissipation of turbulent kinetic energy. k and ε are computed throughout the flow field by solving the following partial differential equations:

$$\frac{\partial(\bar{\rho}k)}{\partial t}+\frac{\partial(\bar{\rho}\tilde{u}_j k)}{\partial x_j}=\bar{\rho}P-\bar{\rho}\varepsilon+\frac{\partial}{\partial x_j}\left[\frac{(\bar{\mu}+\mu_t)}{\sigma_k}\frac{\partial k}{\partial x_j}\right]$$

$$\frac{\partial(\bar{\rho}\varepsilon)}{\partial t}+\frac{\partial(\bar{\rho}\tilde{u}_j\varepsilon)}{\partial x_j}=C_{\varepsilon_1}\frac{\bar{\rho}P\varepsilon}{k}-C_{\varepsilon_2}\frac{\bar{\rho}\varepsilon^2}{k}+\frac{\partial}{\partial x_j}\left[\frac{(\bar{\mu}+\mu_t)}{\sigma_\varepsilon}\frac{\partial \varepsilon}{\partial x_j}\right]$$

where P is the production of turbulence and is given by

$$P = \nu_t \left(\frac{\partial \tilde{u}_i}{\partial x_j} + \frac{\partial \tilde{u}_j}{\partial x_i} - \frac{2}{3} \frac{\partial \tilde{u}_m}{\partial x_m} \delta_{ij} \right) \frac{\partial \tilde{u}_i}{\partial x_j} - \frac{2}{3} k \frac{\partial \tilde{u}_m}{\partial x_m}$$

The values of the empirical coefficients are

$$C_\mu = 0.09 \; ; \; C_{\varepsilon_1} = 1.44 \; ; \; C_{\varepsilon_2} = 1.92 \; ; \; \sigma_k = 1. \; ; \; \sigma_\varepsilon = 1.3$$

The turbulent viscosity, given by $\nu_t = \left(C_\mu k^2 \right) / \varepsilon$, provides the coupling of the turbulence model to the Navier-Stokes, energy, and reacting flow equations. For high speed flows it is well known that the rate of turbulent dissipation decreases as the convective Mach number increases. If this effect is not included in the k-ε model, then high speed turbulent jets are predicted to decay more rapidly than observed in experiments. The method of Sarkar [15] is used to modify the k-ε model for compressibility effects.

The partial differential equations for k and ε are known to be mathematically stiff, that is, they produce rapidly varying values for k and ε near solid walls but have little variation away from a wall. This stiff characteristic couples with the gas dynamics equations and the equations become difficult to solve. To avoid this problem, some turbulence models use wall functions which approximate k and ε near solid walls. These wall functions have proven to be quite sensitive to the near wall pressure gradient and, therefore, unreliable except in simple flows.

Chemical Reaction Modeling. Modeling of the chemical reactions also involves complex physics, similar to the modeling of turbulence. To make the chemistry modeling tractable, it is assumed that the chemical reaction rates are much faster than the time scales associated with the gas dynamic time scales. This assumption allows one to use equilibrium chemistry modeling. For the pre-mixed stream of oxygen and propylene this results in an instantaneous reaction of the fuel and oxidizer as soon as the stream enters the aircap. For the typical pressures that exist in HVOF torches (3-5 atmospheres) the assumption of equilibrium chemistry is a good approximation.

A full equilibrium chemistry model computes the gas species at each cell in the computational domain using the local temperature and pressure and minimizing the Gibbs free energy. This type calculation is computationally intensive and it also tends to strongly couple the flow solution to the chemistry modeling near the inlet of premixed streams. This approach was attempted for the present simulation but numerical instabilities were encountered near the inlet of the premixed streams due to the strong coupling.

An approximate equilibrium chemistry model was used which yields the correct maximum temperature of the combusted mixture and takes into account the dissociation of the gaseous products. If dissociation of the species is not included in the chemistry model then the temperatures

predicted will be unrealistically high, roughly by a factor of two for the present fuel and oxygen reactants. The approximate equilibrium chemistry model is referred to as the instantaneous chemistry model. In this model the reaction is assumed to go to completion immediately upon entering the computational domain, that is, given the inflow temperature and pressure of the pre-mixed gases it is assumed the reaction goes to completion at an infinitely fast rate. Given the oxygen/fuel mixture ratio (near the stocihimetric value of 4.5) the product species that result and their concentrations are determined from the One-Dimensional Equilibrium Chemistry code developed by Gordon and McBride [16]. The pressure and temperature specified for the One-Dimensional Equilibrium code approximate the inflow conditions of the pre-mixed fuel and oxygen stream. It was found from this equlibrium calculation that at the specified initial temperature and pressure excess oxygen remained. The excess oxygen was removed from the reaction equation and the result, written in moles, is

$$C_3H_6 + 3.552\,O_2 \rightarrow 1.036\,CO_2 + 1.964\,CO + 0.441\,H + 0.476\,H_2 + 1.937\,H_2O + 0.398\,O + 0.734\,OH$$

Flow mixtures entering the flow domain are monitored using mixture fractions. A mixture fraction of a given composition at any point in the flow field is defined as the mass fraction of that composition. Since the mixture fraction is a scalar that is transported by the processes of convection and diffusion, the following convection-diffusion equation governs the transport of mixture fraction.

$$\frac{\partial(\rho f_k)}{\partial t} + \frac{\partial(\rho u_j f_k)}{\partial x_j} = \frac{\partial}{\partial x_j}\left[\left(\frac{\mu}{\sigma} + \frac{\mu_t}{\sigma_t}\right)\frac{\partial f_k}{\partial x_j}\right]$$

For most turbulent flows at moderate to high Reynolds numbers, the effect of mass diffusivity among different species is negligible compared to convective transport.

Solid/Liquid Particle Modeling. The particle equations, for either solid or liquid particles, are solved in a Lagrangian frame of reference moving with the particles. The solutions to these equations are used to calculate the source/sink terms for the corresponding gas phase equations. The equation of motion for the particle is written as [17]

$$m_p\frac{d\mathbf{V}_p}{dt} = \frac{1}{2}\rho A_p C_d\left(\mathbf{U} - \mathbf{V}_p\right)\left|\mathbf{U} - \mathbf{V}_p\right| - \mathbf{V}_p\,\nabla p + m_p\mathbf{g}$$

where m_d is the mass of the particle and $\mathbf{V}_p$ is the velocity vector of the particle. C_D is the drag coefficient , and ρ, $\mathbf{V}$, and p are the density, velocity and pressure of the gas, respectively. A_p is the droplet surface area, V_p is the particle volume and $\mathbf{g}$ is the gravity vector. All particles, solid or liquid, are assumed to be spherical. Equation (?) accounts for the acceleration/deceleration of the

droplet due to combined effects of drag from the gas flow, local pressure gradients in the gas, and the body force due to gravity.

The drag coefficient for the particle is based on the local Reynolds number of the particle and is evaluated as

$$R_e = \frac{\rho \left| U - V_p \right| d_p}{\mu}$$

where μ is the molecular viscosity of the gas. The following correlations have been found to be valid for a wide range of Reynolds numbers [17]

$$C_d = \left\{ \begin{array}{ll} \frac{24}{R_e} & \text{for } R_e < 1 \\ \frac{24}{R_e}\left(1 + 0.15 R_e^{0.687}\right) & \text{for } 1 < R_e < 10^3 \\ 0.44 & \text{for } R_e > 10^3 \end{array} \right\}$$

The energy equation for the particle is written as

$$m_p \left(C_p\right)_p \frac{dT_p}{dt} = \pi d^2 \dot{q} - \dot{m}_{ev} L$$

where $\dot{q}$ is the sensible heat transferred to the particle and T_p is the particle temperature. L is the latent heat of vaporization for the droplet fluid and $\left(C_p\right)_p$ is the specific heat of the droplet. $\dot{q}$ is calculated from

$$\dot{q} = \frac{2\kappa \left(T - T_p\right) Nu \ln\left(1 + B_m\right)}{d_p B_m}$$

where κ and T are the thermal conductivity and the temperature of the gas, respectively. Nu is the Nusselt number and it is obtained from the following correlation

$$Nu = 1 + 0.3 Re_p^{0.5} Pr_p^{0.333}$$

where Pr is the Prandtl number of the liquid particle. Bm is the Spalding number and it is computed from

$$Bm_p = \frac{Y_v - Y_\infty}{1 - Y_v}$$

where Y_v and Y_∞ are vapor mass fractions at the liquid droplet surface and the free stream, respectively.

Numerical Solution Technique

Finite Volume Approximations. The discretization of the above differential equations is carried out using a finite-volume approach. First, the solution domain is divided into a large number of discrete volumes or "cells," where all dependent flow variables and space transformation variables are stored at their geometric centers. The finite-volume approach is used because of its attractive capability of conserving flow quantities locally and globally. A co-located, or non-staggered, grid technique is used, that is, the average value of any flow quantity within a control volume is given by its value at each cell center. The finite-volume numerical method essentially involves the integration of the gas dynamic, turbulence model, and species transport equation over each control volume.

The general form of the algebraic (discrete) equations for conservation of a dependent variable ϕ in a finite volume p is given by

$$A_p\phi_p = \sum_{nb} A_{nb}\phi_{nb} + S$$

The coefficients A_{nb} contain both convective and diffusive fluxes and "*nb*" refers to all the neighbors of cell p in a general body-fitted coordinate system. For two-dimensional problems the differencing stencil involves 9 cells, whereas in three-dimensions it involves 19 cells. Because the independent variables are available only at the cell centers, the cell-face values need to be interpolated. For the diffusion terms the value at the cell faces are determined by averaging the two adjacent cells. This results in a second order accurate central difference scheme. For the convection terms the computer code has several options. Typical among them are first-order upwind scheme, a second-order upwind scheme, and the Osher-Chakravarthy scheme. The second-order upwind scheme was used for all simulations presented here.

The continuity equation needs special treatment to resolve the velocity-pressure coupling to overcome the well known checkerboard instability problem. As the fluid density and velocities are available only at cell centers, cell faced values need to be determined from cell-centered values. Linear interpolation between cell centers decouples the velocity and pressure fields giving rise to the checkerboard instability.This instability is eliminated by using a procedure suggested by Rhie and Chow [18]. In this method, the cell-face mass flux is evaluated by averaging the momentum equation to the cell faces and relating the cell face velocity directly to the local pressure gradient. As a result, a fourth-order pressure damping term appears in the discrete form of the continuity equation.

Boundary Conditions and Grid Geometry. Figure 2 shows the computational

domain for both the internal and external flow of the HVOF torch, along with the boundary conditions. The aircap generates a conically converging flow, with a 5° half-angle, and an exit radius of 3.625 mm. The distance from the face of the nozzle, where all of the gases and powder are injected, to the exit plane of the aircap is 10 mm. The nozzle injects solid phase, spherical copper particles with a diameter of 30 μm using Argon as a carrier gas through a circular tube with a radius of 1.5 mm. Pre-mixed propylene (propene) and oxygen are injected through an annulus of width 0.5 mm and an inner radius of 2.5 mm. Air is injected through an annulus of width 1.0 mm and an inner radius of 3.5 mm. Both the oxy-fuel and air are injected at an angle of 5° to the centerline of the torch, i. e., parallel to the surface of the aircap. All solid walls are assumed to be at a fixed temperature of 60 °C.

The mass flow rate of each injectant is given as:

$$\dot{m}_{argon} = 5.613 \times 10^{-4} \text{ kg/sec} = 42.4 \text{ Std ft}^3\text{/hr}$$
$$\dot{m}_{copper} = 5.0 \times 10^{-4} \text{ kg/sec} = 30 \text{ g/min}$$
$$\dot{m}_{propylene} = 1.116 \times 10^{-3} \text{ kg/sec} = 80 \text{ Std ft}^3\text{/hr}$$
$$\dot{m}_{oxygen} = 3.561 \times 10^{-3} \text{ kg/sec} = 340 \text{ Std ft}^3\text{/hr}$$
$$\dot{m}_{air} = 11.39 \times 10^{-3} \text{ kg/sec} = 1200 \text{ Std ft}^3\text{/hr}$$

As can be seen from these flow rates, the fuel-to-oxygen mixture ratio is 3.19. This is less than the stoichiometric ratio of 4.5 because oxygen from the air stream is also consumed in the combustion process. Also noted from the mass flow rate data is that the mass loading of the copper particles, i. e., the dispersed phase, to the total gas flow is 3%. For low mass loading such as this one can ignore volumetric effects of the dispersed phase on the gaseous phase. All injectants are assumed to be at a temperature of 40 °C and the gas flows are assumed to be turbulent.

The HVOF torch is assumed to exhaust into air at a temperature of 30 °C and a pressure of 14.7 psia (Fig. 2b). Air is assumed to be quiescent, except for the flow induced by the supersonic exhaust of the torch. As a result, air is entrained through the upper boundary of the computational domain and part of the down stream boundary. The velocity distribution of the air pumped in along the top boundary of the computational domain is determined by the numerical solution. The outflow boundary of the computational domain is defined to be 20 aircap exit radii from the exit plane of the torch.

As an axisymmetric flow has been assumed, the computational grid need only encompass one-half, for example the upper half, of the physical domain of the torch. The computational grid inside the aircap is composed of 70 axial cells and and 48 radial cells (Fig. 3a). The computational grid outside the aircap is composed of 80 axial cells and 100 radial cells (Fig. 3b). The total number of grid cells for the solution is 11,360. Inside the torch the grid is uniformly spaced in the radial direction and is clustered in the axial direction. The ratio of the cell length (0.15 mm) at the exit plane of the aircap to a cell length (0.05 mm) at the nozzle face is 3. Outside of the torch the grid is highly clustered in both the radial and axial directions. The ratio of the cell height (1.0 mm)

at the upper inflow boundary to the cell height (0.07 mm) on the centerline is 14. The ratio of the cell length (1.5 mm) at the right outflow boundary to the cell length (0.15 mm) at the exit plane of the aircap is 10.

Iterative Solution Procedure. CFD-ACE uses an iterative, segregated solution method wherein the equation sets for each variable are solved sequentially and repeatedly until a converged solution is obtained. The overall solution procedure used is an extension of the SIMPLEC method. SIMPLEC, which stands for "Semi-Implicit Method for Pressure-Linked Equations Consistent," was first proposed by Van Doormal and Raithby [19]. The overall solution procedure for the SIMPLEC algorithm is shown in Fig. 4. Three iteration parameters are specified by the user. T_STEP is the number of time steps, or global iteration steps, required for the simulation. N_ITER is the number of sub-time-step iterations needed for numerical stability or time step accuracy. C_ITER is the number of continuity and pressure correction iterations needed for stability or time accuracy. Typical values for the sub-time-step iterations for the present simulation were N_ITER = 3 and C_ITER = 5. If a steady-state solution is needed, as in the present simulation, N_ITER and C_ITER are kept as small as possible because time accuracy is not needed and only numerical stability of the convergence procedure is required.

The "Solve" blocks shown in Fig. 4 involve the solution of large systems of simultaneous linear equations. These systems are referred to as "sparse" linear systems because the coefficient matrix has non-zero elements only near the main diagonal of the matrix. Iterative equation solvers are preferred for the solution because they are more economical in terms of memory requirements than direct solvers. The linear equation solver used for the present simulations is a type of "whole field" solver which is a modified version of the Strongly Implicit Procedure (SIP) of Stone [20].

Initial Conditions and Iterative Convergence. The initial conditions are the values of all dependent variables in each cell in the computational domain for the first step of the iterative, or time stepping, procedure. Although the values chosen are unimportant with respect to the final converged solution, they are important with regard to the speed with which the solution converges. For the first solution obtained, uniform flow with a constant temperature throughout was assumed. After various trial solutions were obtained, these converged solutions were used for initial solutions for more refined later solutions.

Iterative convergence is determined by the decrease in the magnitude of the sum of the squares of the residuals over the entire computational domain. The residual at a cell is defined as the difference between the value of a given dependent variable at the present iteration and the previous iteration. All solutions presented here have a minimum of five orders of magnitude decrease in the sum of the residuals for all dependent variables; u and v velocity components, static pressure, total enthalpy, turbulent kinetic energy, and the turbulent rate of dissipated energy. The number of iterations required for solution convergence varied from 3,000 to 5,000 time steps, depending on the accuracy of the initial conditions.

Computer Resources Required. All solutions were computed using the UNIX operating system on scientific workstations. Solutions on a Sun Microsystems Sparc 10 model 30

required 10 - 15 hours when the copper particles were not included, that is, when only the gas phase was computed. When eight packets of particles were included, the solutions required 25 - 30 hours of total CPU time. Although these CPU times were typical, little effort was made toward minimizing the computer time by choosing optimum relaxation factors as the solution converged. The computer memory required for solutions was roughly 20 MegaBytes. If this amount of memory is not available in RAM memory, a significant increase in convergence time occurs because the CPU is idle while the RAM memory is swapped back and forth to disk storage.

Summary and Conclusions

During the last few years the thermal spray community has seen new experimental and computational approaches and viewpoints. Researchers from aerospace and defense applications have begun applying their efforts to the topic of thermal spraying. In addition, many of these researchers come from a background in gas dynamics, heat transfer and two-phase flow thereby adding a new perspective to the strongly interdisciplinary field of thermal spraying. HVOF thermal spraying has much in common with computational techniques that have been developed for liquid and solid rocket motors. Although the physical size of the HVOF device is typically much smaller than rocket motors, the gas dynamics, heat transfer, and two-phase flow principals are identical.

The present paper describes the mathematical and numerical formulation of the solution of the flow field in an HVOF thermal spray torch using the computer code CFD-ACE. This code was originally developed for rocket engines and gas turbine engines, although it is also applicable to thermal spraying. Computational results and discussion are given a companion paper [10].

Acknowledgement

We would like to thank Fritz Owens and Anantha Krishnan of CFD Research Corp. for their technical assistance and consultations. We also thank Amalia Lopez of Sandia National Laboratories for her generous assistance.

References

1. Kowalsky, K. A., D. R. Marantz, M. F. Smith, and W. L. Oberkampf, "HVOF: Particle, Flame Diagnostics and Coating Characteristics," Proceedings of the 3rd National Thermal Spray Conf., Long Beach, CA, May, 1990, 587-592.
2. Hackett, C. M., G. S. Settles, and J. D. Miller, "On the Gas Dynamics of HVOF Thermal Sprays," Proceedings of the 6th National Thermal Spray Conf., Anaheim, CA, June, 1993, 167-172.
3. Thorpe, M. L. and H. H. Richter, "A Pragmatic Analysis and Comparison of the HVOF Process," International Thermal Spray Conf., Orlando, FL, May, 1992, 137-147.

4. Ramshaw, J. D. and C. H. Chang, "Computational Fluid Dynamics Modeling of Multicomponent Thermal Plasmas," *Plasma Chemistry and Plasma Processing*, Vol. 12, No. 3, 299-325, (1992).
5. Chang, C. H., "Numerical Simulation of Alumina Spraying in an Argon-Helium Plasma Jet," International Thermal Spray Conf., Orlando, FL, May, 1992, 793-798.
6. El-Haggar, S. M. and C. T. Crowe, "A Two-Dimensional Spray Model for the Spray-Casting Process," Paper No. 93-FE-4, ASME Fluids Engineering Conf., Washington, D.C., June, 1993.
7. Berry, R. A., H. J. Gibeling, and F. J. de Jong, "Multidimensional Calculation of Two-Phase Flow in a Spray-Forming Nozzle Using Eulerian-Lagrangian Analysis,"Paper No. 93-FE-1, ASME Fluids Engineering Conf., Washington, D.C., June, 1993.
8. Power, G. D., T. J. Barber, and L. M. Chiappetta, "Analysis of a High Velocity Oxygen-Fuel (HVOF) Thermal Torch," AIAA Paper No. 92-3598, AIAA/SAE/ASME/ASEE 28th Joint Propulsion Conf., Nashville, TN, July, 1993.
9. Smith, E. B., G. D. Power, T. J. Barber, and L. M. Chiappetta, "Application of Computational Fluid Dynamics to the HVOF Thermal Spray Gun," International Thermal Spray Conf., Orlando, FL, May, 1992, 805-810.
10. Oberkampf, W. L. and M. Talpallikar, "Analysis of a High Velocity Oxygen-Fuel (HVOF) Thermal Torch, Part 2: Computational Results," Proceedings of the 7th National Thermal Spray Conf., Boston, MA, June, 1994.
11. Lai, Y. G., A. J. Przekwas and R. M. C. So, "Aerodynamic Flow Simulation Using a Pressure-Based Method and a Two-Equation Turbulence Model," AIAA Paper No. 93-2902, AIAA 24th Fluid Dynamics Conf., Orlando, FL, July, 1993.
12. Jiang, Y., Y. G. Lai, S. Y. Ho and A. J. Przekwas, "3D Simulations of Complex Flows with an Implicit Mulit-Domain Approach," AIAA Paper No. 93-3124, AIAA 24th Fluid Dynamics Conf., Orlando, FL, July, 1993.
13. "Numerical Grid Generation," ed. J. F. Thompson, Elsevier Sci. Pub., (1982).
14. Launder, B. E. and D. B. Spalding, "The Numerical Calculation fo Turbulent Flows," *Computational Methods Applied to Mechanics and Engineering*, Vol. 3, 269-289, (1974).
15. Sarkar, S. "The Analysis and Modeling of Dilatational Terms in Compressible Turbulence," *J. of Fluid Mechanics*, Vol. 227, 473-493, (1991).
16. Gordon, S. and B. J. McBride, "Computer Program for Calculation of Complex Chemical Equilibrium Compositions, Rocket Performance, Incident and Reflected Shocks, and Chapman-Jonquet Detonations," NASA SP-273, (1976), new version (1989).
17. Crowe, C. T., M. P. Sharma and D. E. Stock, "The Particle-Source-in Cell (PSI-DELL) Model for Gas-Droplet Flows," *J. of Fluids Engineering*, Vol. ?, No. ?, 325-332, (1977).
18. Rhie, C. M. and W. L. Chow, "Numerical Study of the Turbulent Flow Past an Airfoil with Trailing Edge Separation," *AIAA J.*, Vol. ?, No.?, 1525-1532, (1983).
19. Van Doormaal, J. P. and G. D. Raithby, "Enhancements of the SIMPLE Method for Predicting Incompressible Fluid Flows," *Numerical Heat Transfer*, Vol. ?, No. ?, 147-163,

(1984).

20. Stone, H. L., "Iterative Solution of Implicit Approximates of Multi-Dimensional Partial Differential Equations," *SIAM J. Numerical Analysis*, Vol. 5, No. ?, 530-558, (1968).

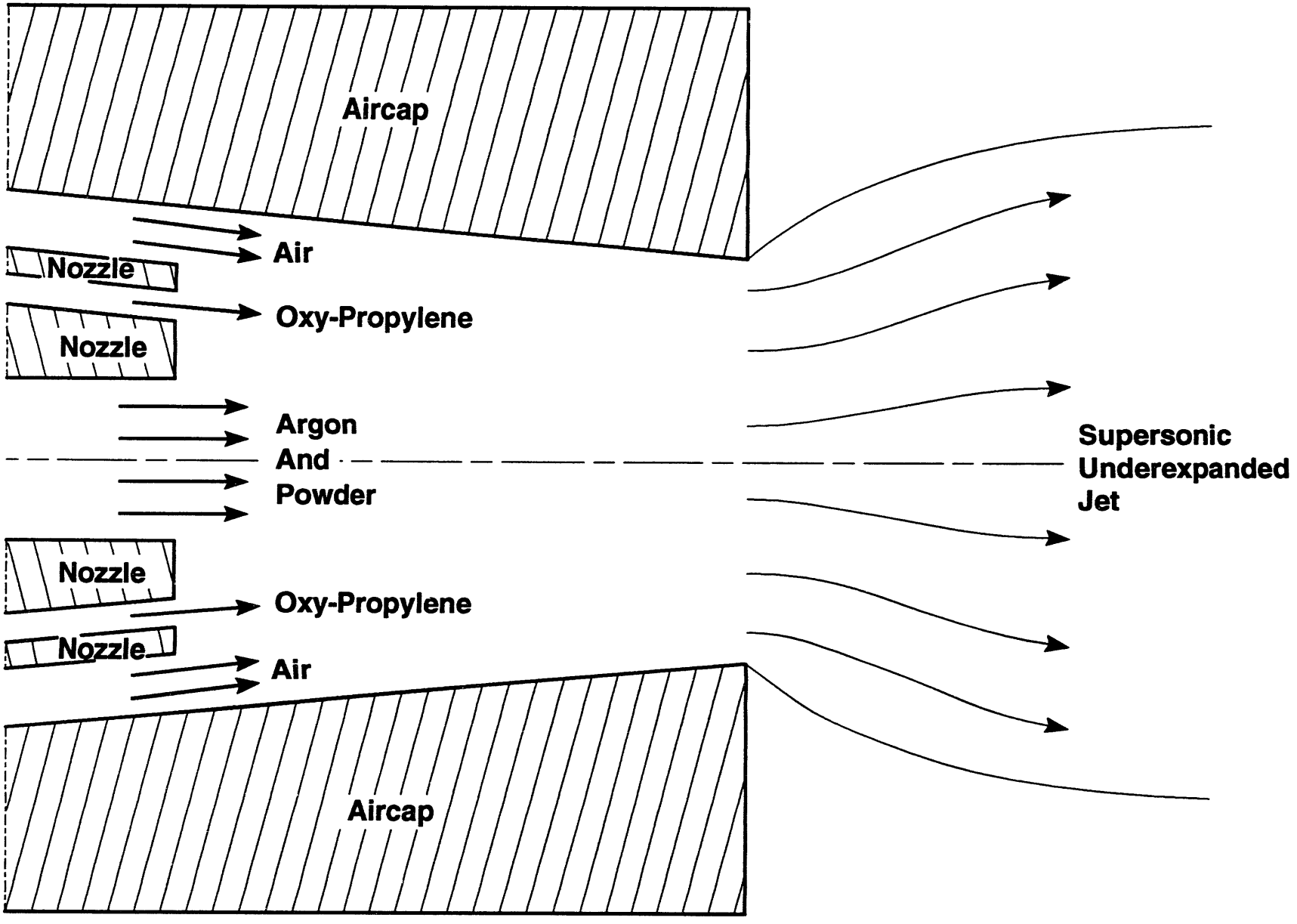

Figure 1: Schematic of HVOF Thermal Spray Torch

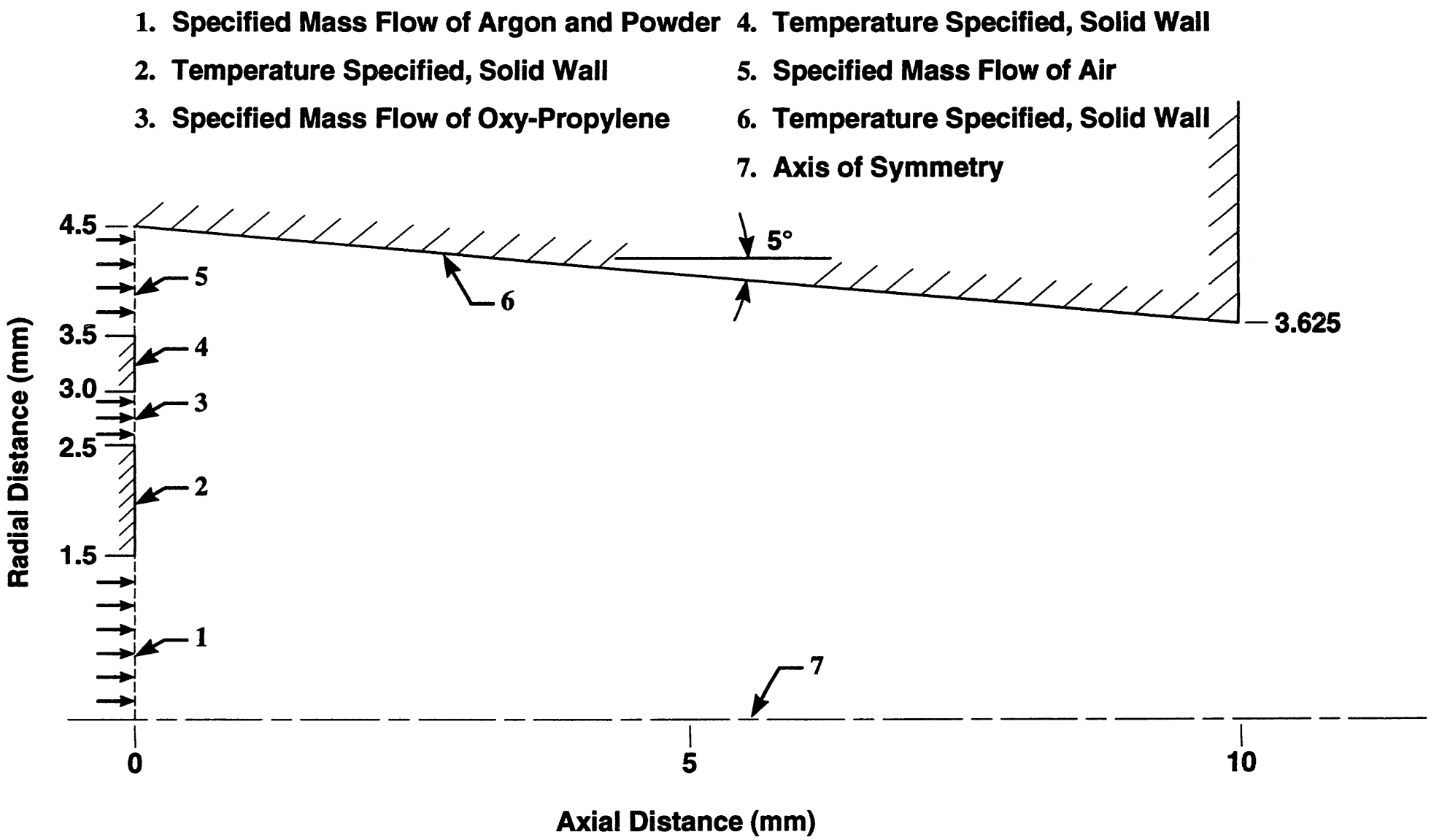

Figure 2a: Computational Domain and Boundary Conditions Inside Torch

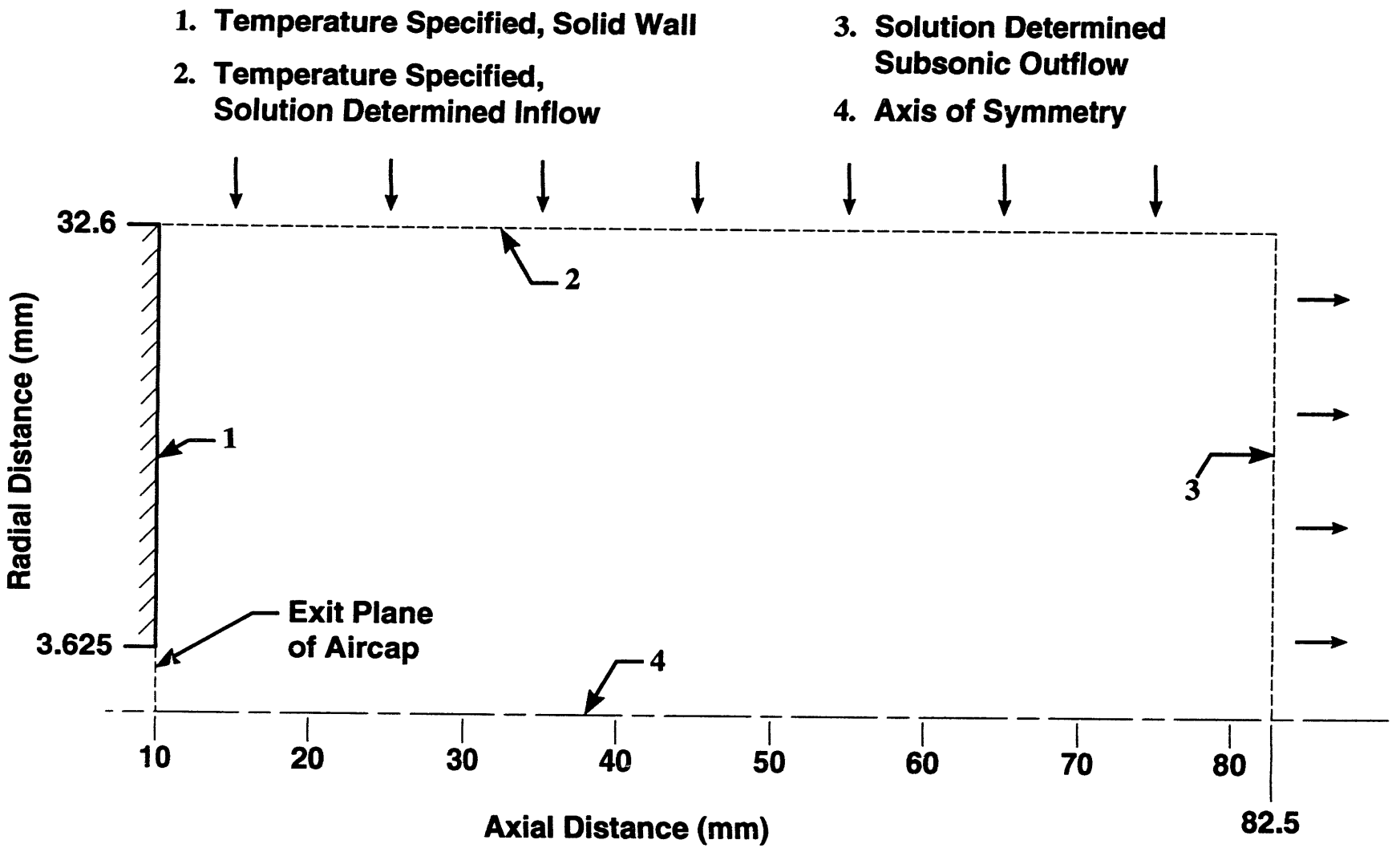

Figure 2b: Computational Domain and Boundary Conditions Outside Torch

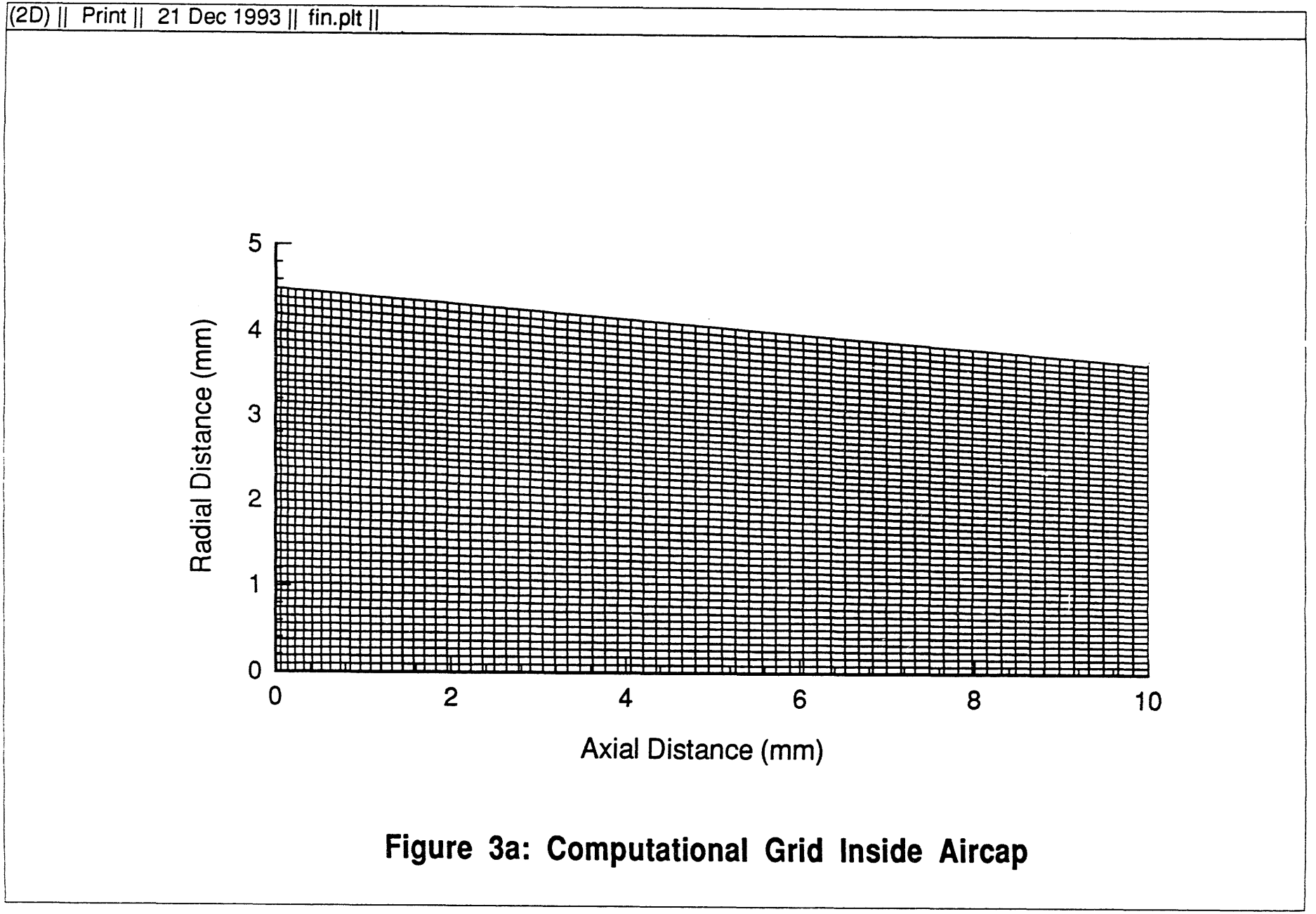

Figure 3a: Computational Grid Inside Aircap

Figure 3b: Computational Grid Outside Aircap

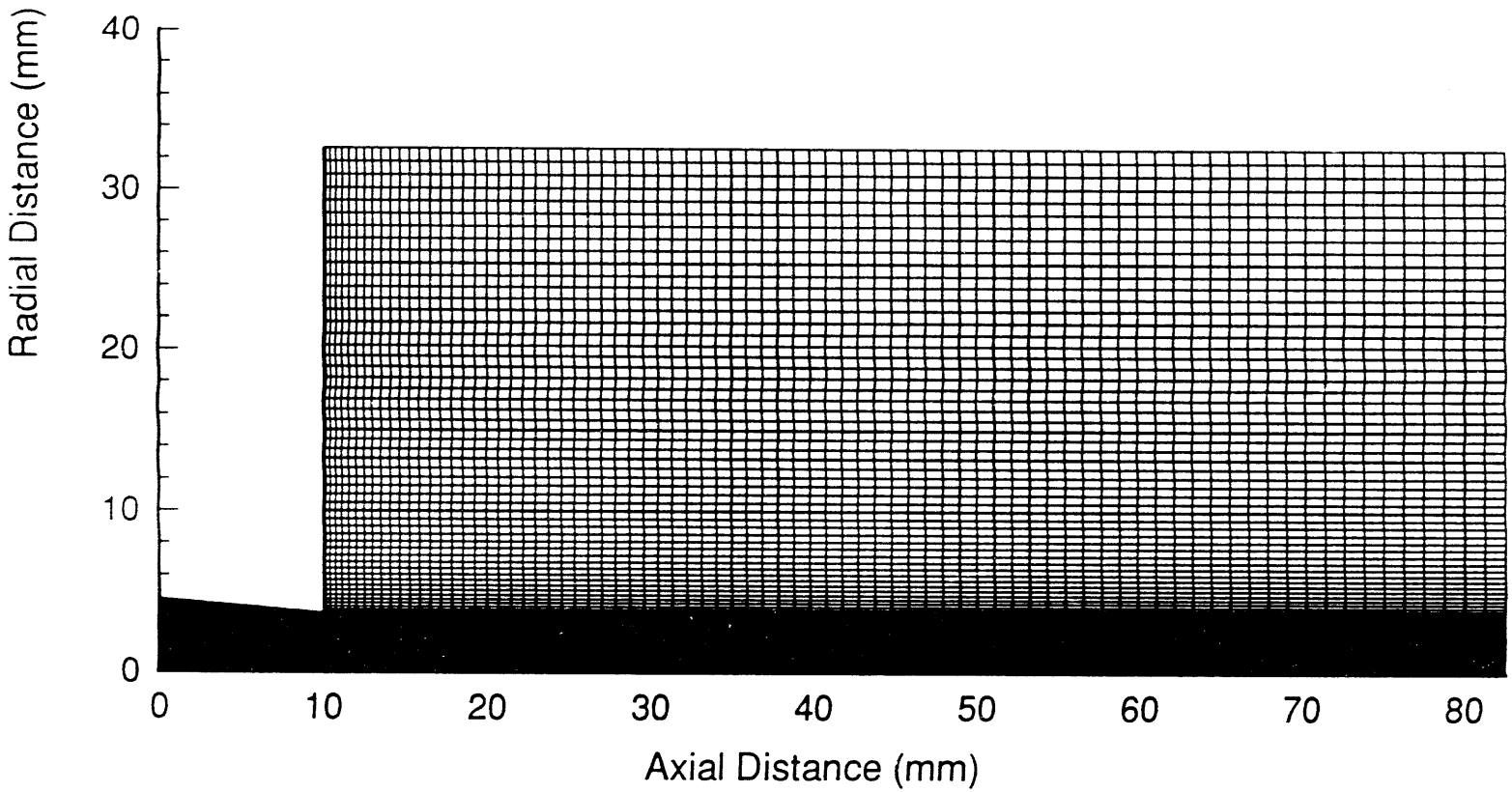

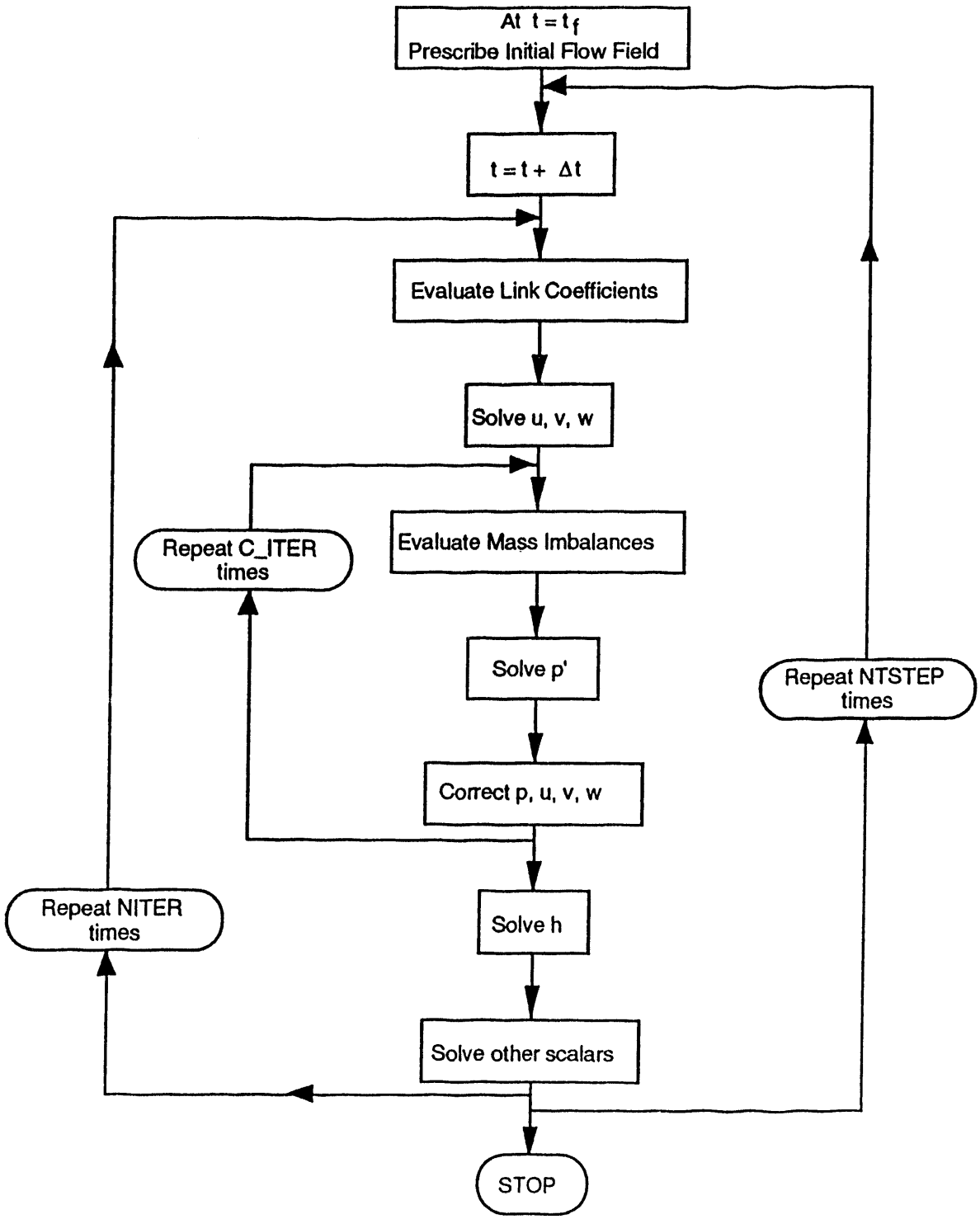

Figure 4: Iterative Convergence Procedure

END

DATE
FILMED
5/13/94